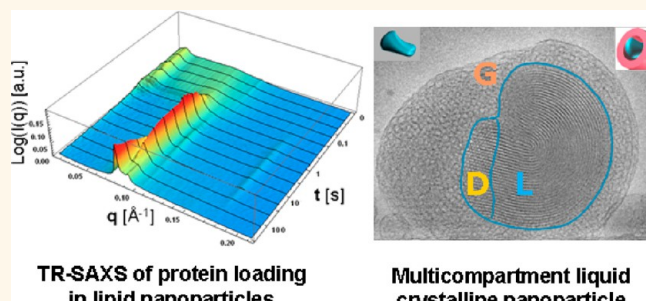


# Multicompartment Lipid Cubic Nanoparticles with High Protein Upload: Millisecond Dynamics of Formation

Borislav Angelov,<sup>†</sup> Angelina Angelova,<sup>‡,\*</sup> Sergey K. Filippov,<sup>†</sup> Markus Drechsler,<sup>§</sup> Petr Štěpánek,<sup>†</sup> and Sylviane Lesieur<sup>‡</sup>

<sup>†</sup>Institute of Macromolecular Chemistry, Academy of Sciences of the Czech Republic, Heyrovsky Sq. 2, CZ-16206 Prague, Czech Republic, <sup>‡</sup>CNRS UMR8612 Institut Galien Paris-Sud, Université Paris Sud 11, F-92296 Châtenay-Malabry, France, and <sup>§</sup>Laboratory for Soft Matter Electron Microscopy, Bayreuth Institute of Macromolecular Research, University of Bayreuth, D-95440 Bayreuth, Germany

**ABSTRACT** Membrane shapes, produced by dynamically assembled lipid/protein architectures, are crucial for both physiological functions and the design of therapeutic nanotechnologies. Here we investigate the dynamics of lipid membrane–neurotrophic BDNF protein complexes formation and ordering in nanoparticles, with the purpose of innovation in nanostructure-based neuroprotection and biomimetic nanoarchitectonics. The kinetic pathway of membrane states associated with rapidly occurring nonequilibrium self-assembled lipid/protein nanoarchitectures was determined by millisecond time-resolved small-angle X-ray scattering (SAXS) at high resolution. The neurotrophin binding and millisecond trafficking along the flexible membranes induced an unusual overlay of channel-network architectures including two coexisting cubic lattices epitaxially connected to lamellar membrane stacks. These time-resolved membrane processes, involving intercalation of discrete stiff proteins in continuous soft membranes, evidence stepwise curvature control mechanisms. The obtained three-phase liquid-crystalline nanoparticles of neurotrophic composition put forward important advancements in multicompartment soft-matter nanostructure design.



TR-SAXS of protein loading in lipid nanoparticles

Multicompartment liquid crystalline nanoparticle

**KEYWORDS:** lipid–protein nanoassembly · dynamic membrane curvature · amphiphile nanoarchitectonics · multicompartment lipid nanoparticle · morphological transition pathway · millisecond time-resolved SAXS · cryo-TEM · BDNF-loaded cubosome

Compartmentalization in biological systems and formation of cubic and tubular membrane architectures in diverse cell types and organelles<sup>1–4</sup> are currently stimulating the research on mesoporous particles of sophisticated shapes and channel organizations.<sup>5–14</sup> Structural knowledge about the dynamics of complex protein/lipid assemblies accelerates the progress in amphiphile nanoarchitectonics and helps to improve the design of synthetic nanomedicine carriers.<sup>15–17</sup> In this perspective, the latest concepts and principles, underlying the biomembrane organization, structural dynamics (deformation, curving, shape transitions, fusion/fission), elasticity, kinetic traps, interaction with guest molecules, and response to external

stimuli,<sup>18–31</sup> offer unexploited possibilities for the creation of self-assembled lipid- and macromolecule-based nanostructured materials with incorporated functionality (e.g., photoreceptor cells, neuroprotective devices, theranostics targeting, nanoarchitectonics, etc.).<sup>32–51</sup>

While the techniques for establishing equilibrium structural packing of proteins in lipid cubic membrane templates have been well recognized,<sup>52</sup> the experimental methods for real-time investigation of the structural pathways, transformation dynamics, and nonequilibrium arrested phases in soft lipid and amphiphile nano-systems<sup>53–63</sup> are yet in development. Millisecond time-resolved (TR) structural investigations of the dynamics of DNA-driven

\* Address correspondence to angelina.angelova@u-psud.fr.

Received for review March 5, 2014 and accepted April 14, 2014.

Published online April 17, 2014  
10.1021/nn5012946

© 2014 American Chemical Society

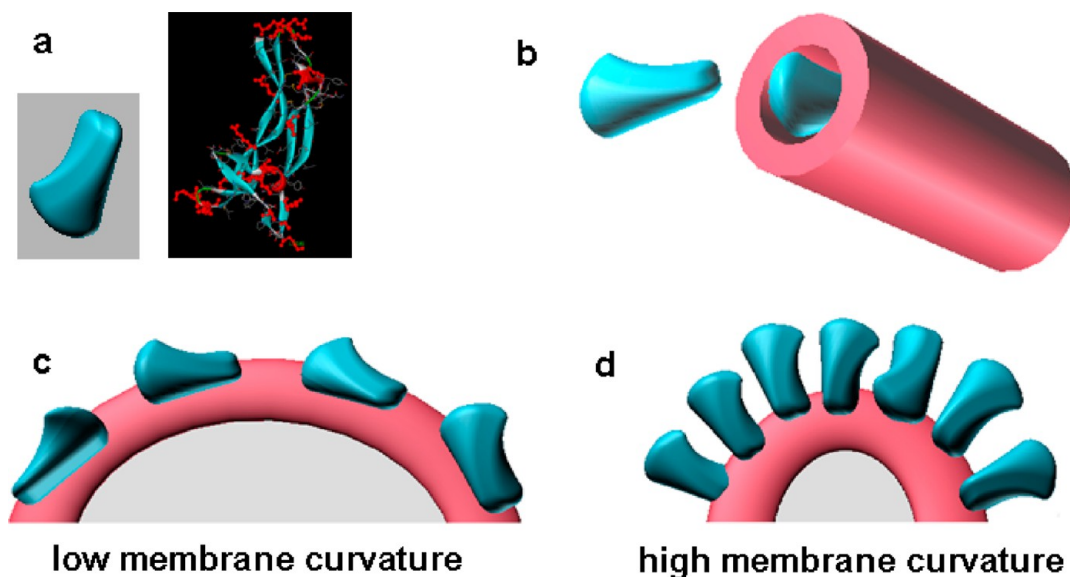


**Figure 1.** Neurotrophin BDNF binding at vesicular membrane/water interfaces, or loading in high-curvature lipid tubes, induces protein-modulated membrane curvature changes. The self-assembled nanosystem involves (a) neurotrophin BDNF (a multivalent macroion with a net positive charge  $Z = +9e$  (basis amino acids marked in red color) and predominantly  $\beta$ -sheet conformation (protein structure displayed using the pdb code: 1BND)); (b) aqueous channels of tubular lipid assemblies for neurotrophin confinement; and vesicular membranes (c,d) (initial state shown in Figure 4a). The curvature of the lipid/water interfaces depends on the coverage of bound proteins. A “side-on” orientation of the BDNF molecules corresponds to low-membrane-curvature particles (c), whereas a crowded state of protein molecules in an “edge-on” orientation at the lipid membrane interfaces (d) may induce a high-curvature cubic membrane structure.

membrane processes<sup>54</sup> have been initiated in parallel with the progress in X-ray scattering studies of protein solutions.<sup>64–66</sup>

Presently, the state-of-the-art highly brilliant TR small-angle X-ray scattering (SAXS) is expected to reveal the protein-induced transient changes in the membrane curvature in real time and the kinetics of short- and long-lived intermediate states in the membrane transformations. Such high resolution experiments may provide insights into temporary-living structures upon protein trafficking and membrane deformations, which are not accessible *via* steady-state microscopy imaging. Moreover, the rate constants of rapid complexation processes can be estimated from the sequence of dynamic roentgenograms.<sup>54</sup> Despite the importance of the molecular details, the structural and kinetic pathways by which soft lipid nanochannel-based carriers<sup>11,14,30</sup> may entrap a neurotrophic protein and may interact with a lipid membrane, in order to transport the beneficial molecule, have not been elucidated yet. The role of membrane curvature in the nanostructure and nanoparticle (NP) interactions with interfaces is another fundamental problem of ongoing interest.<sup>31</sup>

Here we investigate in real time the structural pathway and morphological changes occurring upon nonequilibrium rapid-mixing binding of brain-derived neurotrophic factor (BDNF) (Figure 1a) to bilayer membrane vesicles and lipid architectures of nanochannel organization (Figures 1b–d). The protein dimensions [length  $\sim 4$  nm; diameter  $\sim 3$  nm] are comparable with

the lipid membrane thickness. BDNF, as a member of the neurotrophin family, is studied as a pro-survival signaling molecule of strong ongoing interest for synaptic repair, neuroregeneration, and treatment of psychiatric disorders.<sup>67–70</sup> The neurotrophin-BDNF levels are reduced under pathological conditions (stroke, depression, schizophrenia, post-traumatic stress disorder, amyotrophic lateral sclerosis, multiple sclerosis, Alzheimer disease, etc.).<sup>67–69</sup> Consequently, the protein needs to be locally administered<sup>67</sup> to the relevant target sites in the central nervous system with the purpose to compensate its deficiency. Whereas the biochemical mechanisms of the BDNF action require activation of its membrane receptors,<sup>67,69</sup> the structural basis of the neurotrophin potentiation and the dynamics of the membrane processes related to its trafficking upon local administration have not been previously studied. The reported here novel neurotrophin/lipid architectures, shaped in nanoparticles of ordered three-phase self-assembled inner structures with multiple compartments and stepwise interfacial curvatures, as well as the membrane-nanoparticle structural transitions (studied with exceptional spatial and temporal resolutions) are significant in the context of nanotechnology-based neuroprotective strategies and interaction of soft membranes with rigid protein shapes.

## RESULTS AND DISCUSSION

**Choice of Biomimetic Amphiphilic Compositions.** Lipid assemblies were created with a multicomponent lipid

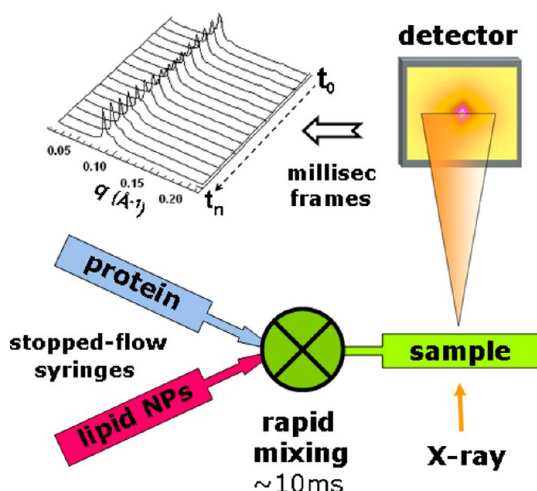


**Figure 2.** Schematic presentation of the principle of the rapid-mixing stopped-flow setup coupled to *in situ* structural SAXS measurements. The synchrotron SAXS patterns are recorded with 4 ms resolution using a 2D detector.

system allowing for a composition-mediated interfacial curvature tuning. The chemical composition comprised the natural lipid molecule eicosapentaenoic acid (EPA), which was studied as a representative  $\omega$ -3 polyunsaturated fatty acid of therapeutic importance for the neurodegenerative and neuropsychiatric diseases.<sup>71</sup> EPA was incorporated in membranous structures of monoolein (MO), a lipid with a propensity to form bicontinuous liquid crystalline architectures preserving the protein structure.<sup>6,11,50,51</sup> An essential property of the polyunsaturated fatty acid, as a negative-curvature lipid, is that it promotes the formation of membrane fusion intermediates and inverted nonlamellar phases. EPA may regulate the membrane elasticity and may favor the bending of the lipid bilayer leaflets toward destabilization of the flat membranes. It imparts a negative charge to the artificially designed membrane interfaces. *In vivo*, EPA may potentiate the neurotrophin BDNF activity by influencing also its signaling pathway.<sup>71</sup>

The created nanoscale lipid membrane assemblies of monoolein and EPA were sterically stabilized against aggregation by PEGylation. The coverage by PEG chains was kept minimal. Every component of the lipid mixture, as well as the PEGylated derivative ( $V_{1000}$ ), gave a contribution to the spontaneous curvature of the self-assembled system, which was studied in a dispersed state in large excess of aqueous phase.

**Real-Time Monitoring of the Millisecond Structural Changes Occurring upon Formation of Lipid Membrane–Protein BDNF Liquid Crystalline Architectures.** The performed time-resolved structural study exploited the advantages of highly brilliant synchrotron SAXS measurements coupled to a rapid-mixing stopped-flow technique as schematically presented in Figure 2. The dynamic membrane processes were comprehensively studied at temporal resolution of 4 ms, which represents a state-of-the-art methodological advance.

The structural pathway of neurotrophin-lipid complexation was determined in real time for a lipid membranous system that mimics the coexistence of diverse vesicular and tubular shapes existing in living matter.<sup>1</sup> The starting state, to which the neurotrophin was administered in order to simulate exogenous protein injection to cellular barriers and vital pores, involved vesicular bilayer membranes (Figures 1 and 4a) and a small amount of lipid architectures with hexagonally packed channels (Figure S1, Supporting Information). In terms of membrane curvature, this initial system of lipid bilayers and tubular monolayer leaflet structural elements represented kinetically stabilized nonequilibrium dispersion of nanoparticles (Figures S2 and S3, Supporting Information). The membrane structures were in a liquid-crystalline fluid phase state and were subjected to stopped-flow rapid mixing with neurotrophic protein solutions (Figure 2). The purpose was to experimentally examine in real time how the signaling protein BDNF influences the membrane structural dynamics, through formation of transient or stable protein–lipid architectures, which may induce remodeling of the membrane interfaces relevant to physiological function or initiation of nanocrystallization.

Sequences of SAXS patterns revealing the dynamics of the structural events and the evolution of the membrane architectures occurring upon rapid mixing of water-soluble protein molecules and flexible membrane structures are presented in Figures 3 and S4 (Supporting Information). The millisecond-range kinetic pathway was determined by analysis of up to 670 SAXS frames recorded in programmed sequences of rapid-mixing shots (see the detailed description of the methods and Figure S4, Supporting Information). The acquired dynamic SAXS patterns revealed that the protein macromolecules were quickly trafficked from the solution phase into the membranous structures, enabling the entrapment of BDNF in a bound state. The data analysis indicates that peaks of an inverted hexagonal  $H_{II}$ -phase are present up to  $t \sim 200$  ms from the beginning of the SAXS measurements (see also Figure S4, Supporting Information, frame 14 of the SAXS scan). The emerging first lamellar peak results from the arrangement of protein–lipid complexes into onion lamellar structures. A lamellar phase forms at  $t \sim 190$  ms (see Figure S4, Supporting Information, frame 10) with Bragg peaks positioned at  $q_1 = 0.088 \text{ Å}^{-1}$  and  $q_2 = 0.176 \text{ Å}^{-1}$ . Protein-induced formation of cubic membrane intermediates is provoked at  $t \sim 120$  ms (see Figure S4, Supporting Information, frame 8). Bragg peaks of two types of bicontinuous cubic lattices are detected (Figure 2, Figure S4, Supporting Information). The flat lamellae are progressively transformed into a cubic membrane architecture, which stably dominates the system at  $t > 57$  s.

Conceptually, the investigated dynamic self-assembly processes at the membrane interfaces are suggested

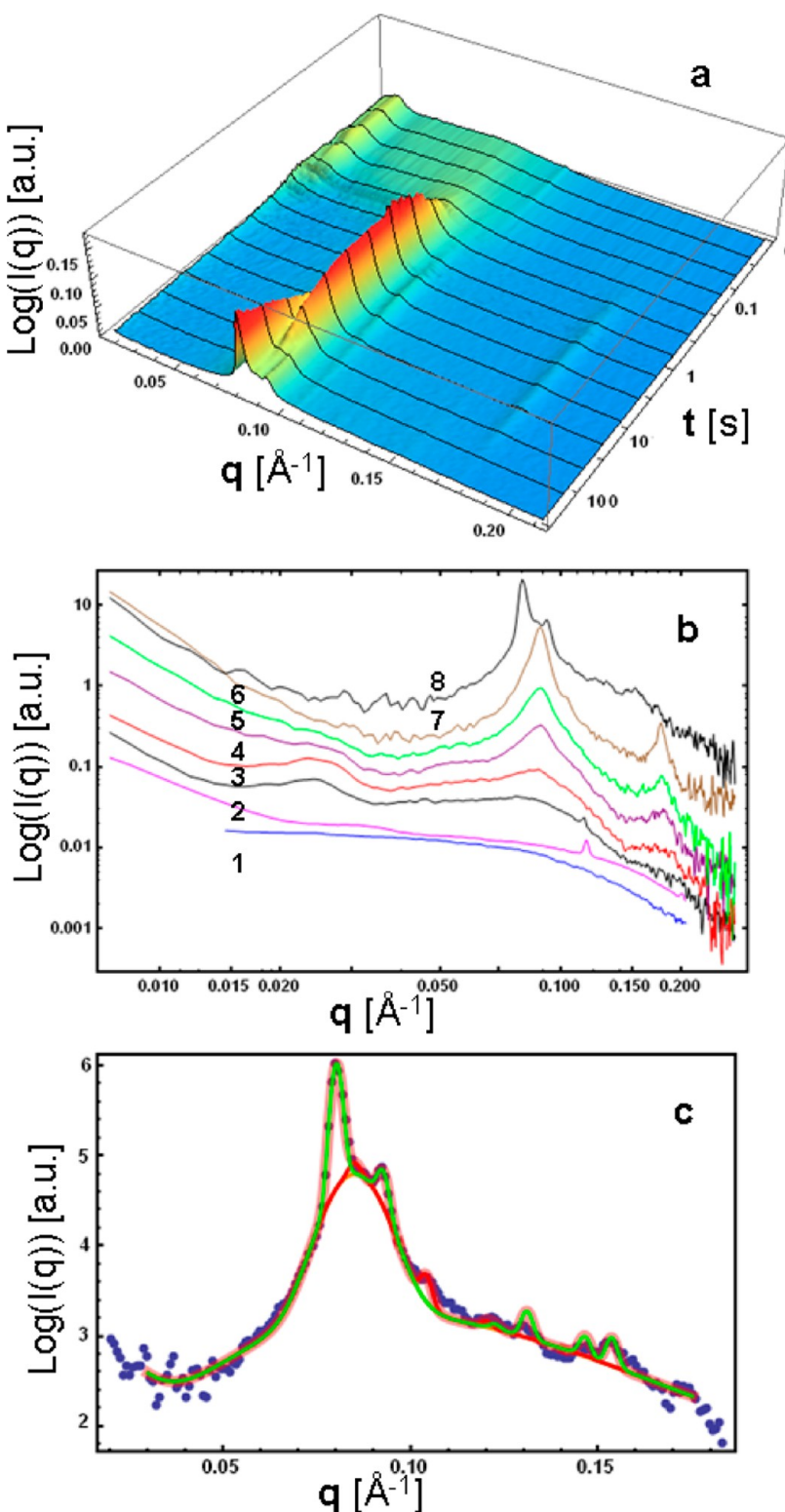
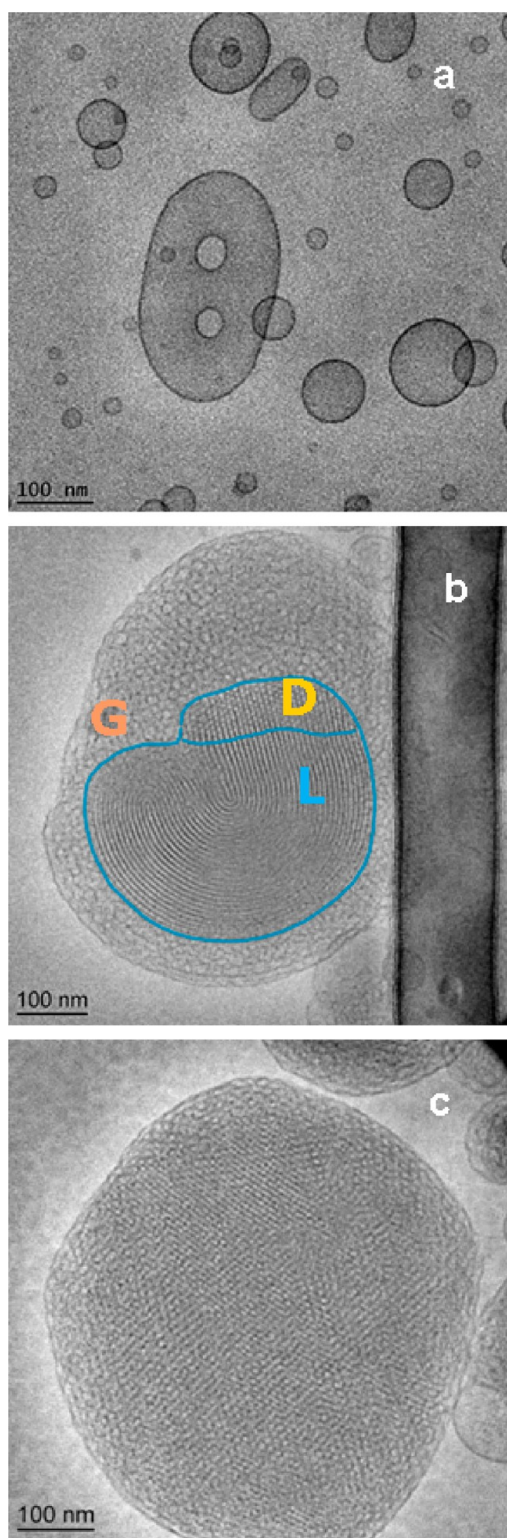


Figure 3. (a) Time-resolved SAXS patterns showing the kinetic pathway of neurotrophin binding and trafficking along the membrane/water interfaces. The membrane structural dynamics are studied by performing sequential rapid-mixing stopped-flow shots, during which SAXS frames are acquired with exposure time of 4 ms. Every shot of rapid mixing involves 75 frames recorded in a geometrical progression. (b) Selected frames of the TR-SAXS scan revealing the key dynamic membrane structures (see the text) induced by neurotrophin binding: curve 1, free protein; curve 2, unloaded lipid system at  $t = 0$  ms; curves 3–7 correspond to the SAXS frames at  $t = 7, 93, 211, 224$ , and 657 ms; and curve 8 is recorded at  $t = 130$  s. (c) Fitting of the experimental data (curve 8 of panel (b)) by coexisting cubic and lamellar structures. The fits for the cubic membranes (observed in (a)) determined bilayer thicknesses in the range from 4.11 to 4.20 nm.

to involve at least three stages: (i) fast electrostatic binding of the positively charged protein molecules to the flexible, negatively charged membrane interfaces accompanied by charge neutralization (rate constant  $k_1$ ); (ii) dynamic formation of intermediate onion lamellar states with modified membrane curvatures and rapid assembly of nanostructured protein/lipid complexes (rate constant  $k_2$ ); (iii) relatively slow remodeling of the kinetically trapped shapes toward equilibrium structures of more ordered or aggregated states (rate constant  $k_3$ ). While stage (i) may occur on the time scale of microseconds and is not directly detectable as a structural change in the SAXS patterns, the millisecond TR-SAXS appears to be an excellent tool for the investigation of stage (ii) of the membrane shaping, thus leaving stage (iii) for structural measurements over seconds. Here, the kinetic pathways presented in Figures 3 and S4 (Supporting Information) characterize the rapidly evolving sequence of intermediate architectures resulting from the membrane curvature changes induced upon protein entrapment in the lipid phase.

The obtained results showed that the protein–lipid complexation occurs through two parallel processes evidenced by (i) the growth of onions from the initial bilayers present in the lipid mixture, and (ii) the  $H_{\parallel}$ -phase peaks vanishing, which characterizes the structural rearrangement of the tubular monolayer lipid population after protein coupling (see also Figure 6 below). The existence of two different kinetic processes is not surprising considering that the protein entry, diffusion, and complexation into the interior of the aqueous channels of the highly curved lipid tubes should be associated with different free energy barriers as compared to the protein surface binding to lower-curvature vesicular membranes. Moreover, binding of the positively charged protein molecules to the anionic groups of the lipid/water interfaces changes the headgroups hydration. Generally, lipid headgroup condensation by multivalent counterions leads to dehydration.

The decreased hydration in the lipid system in response to the protein loading is expected to favor the formation of curved membrane structures. Indeed, the obtained SAXS data demonstrate that the protein intercalation in the lipid lamellae and the lateral repulsion between the charged proteins provoke interfacial trafficking events, which enable a fast rearrangement of the flat membranes into 3D cubic-membrane architectures involving aqueous channels (see Figures 4b,c and 5). The Bragg peak positions in Figure 3b specify a perfect epitaxial relationship between the bicontinuous cubic double diamond  $Pn3m$  ( $q_{110} = 0.085 \text{ \AA}^{-1}$ ) and the onion ( $q_{\text{onion}} = 0.085 \text{ \AA}^{-1}$ ) structures. The estimated cubic lattice parameter after protein upload ( $a_D = 10.45 \text{ nm}$ ) suggests protein confinement in the aqueous channel network. It is remarkable that the cubic lattice needs short times for self-assembly ( $\sim 120 \text{ ms}$ )



**Figure 4.** Cryo-TEM images of (a) initial lipid membranes before BDNF administration, (b) three-phase nanostructure stably formed throughout the BDNF upload in nanocarriers, and (c) BDNF-loaded diamond-type cubosome nanoparticle. The blue line in (b) indicates the domain boundaries between the inner L, D, and G mesophases: L, lamellar  $L_{\alpha}$ ; D, bicontinuous cubic double diamond  $Pn3m$ ; and G, bicontinuous cubic gyroid  $Ia3d$  structure.

because it nucleates and grows from preformed onion membrane intermediates. Thus, the time between the

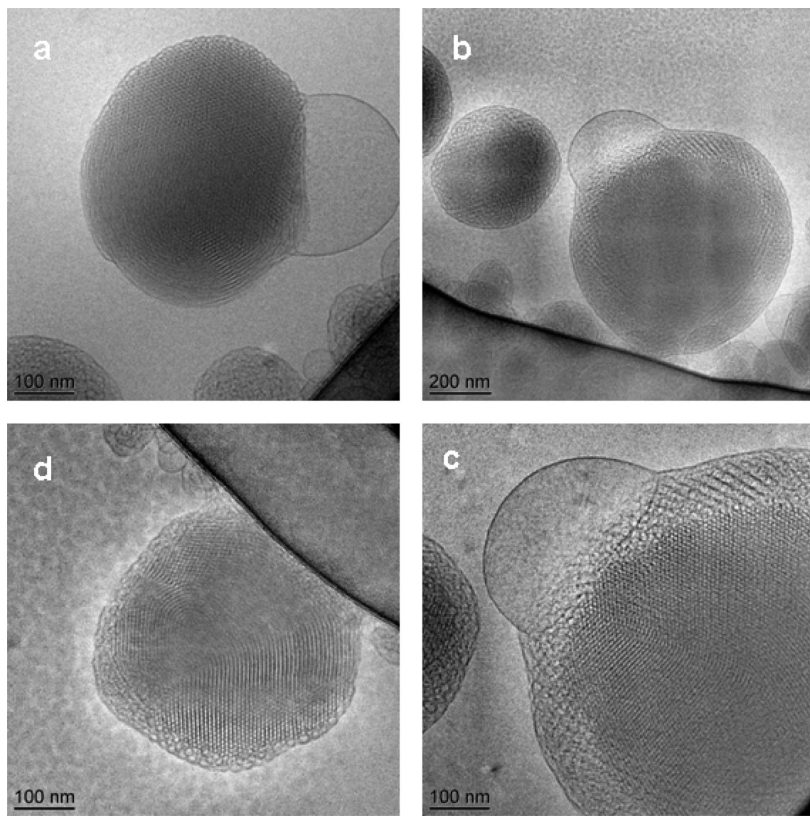


**Figure 5.** Cryo-TEM images demonstrating long-lived intermediate states of the bilayer membrane vesicle-to-cubic membrane transition upon neurotrophic protein trafficking at the lipid/water interfaces and loading in nanochannel-type lipid nanoparticles. The sizes of the bicontinuous cubic and onion-lamellar domains inside the nanoparticles are determined by the quantity of the uploaded protein.

first emergence of the second cubic peak and the second lamellar peak was just about 70 ms.

A bigger bicontinuous cubic lattice emerged in a coexistence with the diamond cubic *Pn3m* and the lamellar structures at  $t \sim 450$  ms of the kinetic pathway. A best fit of the SAXS data was obtained with a gyroid *la3d* structure of a lattice parameter  $a_G = 19.19$  nm. The determined epitaxial ratio between the two cubic lattice parameters is  $a_G/a_D = 1.83$ . The kinetics analysis, performed on the basis of the TR-SAXS patterns, suggests that the gyroid nanophase growth reduces the amount of onions and bilayer membrane fragments in the system. The cubic double diamond *Pn3m* peak intensities remain visibly constant (Figure S4, Supporting Information).

**Three-Phase Nanoarchitectures Resulting from Dynamic Protein Assembly with the Membrane Interfaces and Discrete Jumps of Curvature.** Key events of the nanostructured particle transition pathway occurred also at the following times determined by TR-SAXS: (i) the intensities of the cubic lattice peaks (*Pn3m* (*D*) and *la3d* (*G*)) considerably prevailed over the Bragg peaks of the lamellar structure at  $t \sim 27$  s (Figure S4, Supporting Information); (ii) the larger *la3d* (*G*) cubic lattice dominated over the *Pn3m* (*D*) cubic structure at the final stage (Figure S4, Supporting Information, last frames) as a result of the protein trafficking and complexation at the membrane interfaces. Figure 4b shows a cryo-TEM image of a three-

phase (*L/D/G*) multicompartiment nanoparticle as a steady state reached in the membrane structural transformation. The neurotrophin BDNF loading produces also diamond (*D*) type cubosome nanoparticles as equilibrium liquid crystalline nanostructures (Figure 4c). The entire variety of intermediate states of the investigated kinetic pathway can only be precisely resolved by TR-SAXS (see Figure S4, Supporting Information).

It should be underlined that the cubic lattice does not form directly from the tubular  $H_{\parallel}$  structure. The latter consists of curved lipid monolayer leaflets that must first rearrange into lipid bilayer building blocks before being able to assemble into a bicontinuous cubic membrane. Figure 5 shows cryo-TEM images demonstrating stages of the neurotrophin BDNF-induced vesicle-to-cubosome transition that occurs in the lipid nanoparticles upon interaction with the protein.

**Kinetics of Quantitative Neurotrophin Uptake by Membrane Nanoassemblies.** The time dependence of the scattering intensities (Figure S4, Supporting Information) of the protein-entrapping lipid membrane assemblies vs the scattering of the free protein (BDNF) at a chosen wave vector ( $q$ ) range was used for estimation of the protein percentage trafficked from the injected aqueous solution into the lipid membrane structures. The result is presented in Figure 6. Thus, our TR-SAXS investigation established that 82% of the injected

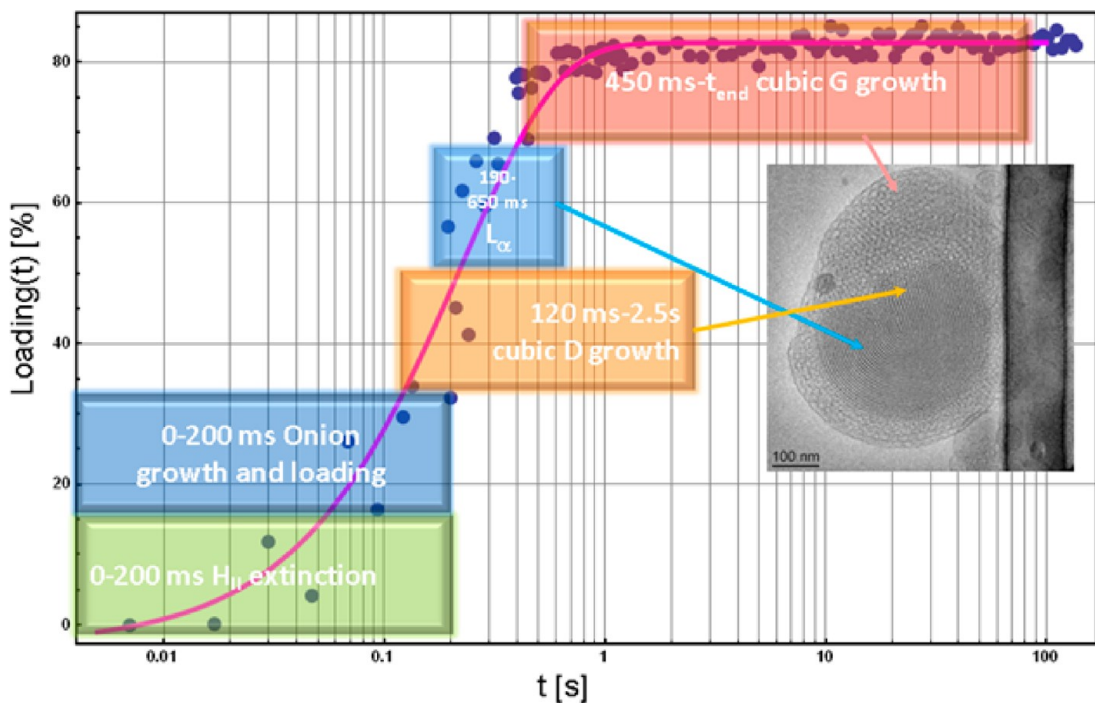


Figure 6. Time dependence of protein loading in lipid nanoarchitectures determined from analysis of the TR-SAXS sequence detailed in Figure S4 (Supporting Information). The rate constant of protein uptake in nanoparticles is determined to be  $4.477 \text{ s}^{-1}$ . The protein loading efficiency increases up to 82% within milliseconds after the protein injection. Abbreviations:  $H_{II}$ , inverted hexagonal structure;  $L_{\alpha}$ , lamellar bilayer structure; D, bicontinuous cubic double diamond ( $Pn3m$ ); and G, bicontinuous cubic gyroid ( $Ia3d$ ) structures.

protein was entrapped in lipid membranous nanostructures and at membrane interfaces within the first second from its administration (see the plateau level in Figure 6). This kinetic result provides a new proof for the high efficiency of the monoolein-based cubic membrane systems and nanoparticles for protein upload, which has previously been attempted with enzymes only under static conditions.<sup>72</sup> We found that the formation of the ordered  $Pn3m$ ,  $L_{\alpha}$ , and  $Ia3d$  phases is triggered at protein loading percentages of about 35, 40, and 70%, respectively (see the diagrams in Figure 6).

The performed TR-SAXS study provided experimental evidence, at exceptional spatial and temporal resolution, for the induction of transient curvature alterations in the lipid membrane architectures upon protein (BDNF) anchoring and loading into the nanochannel network systems. The kinetic pathway revealed the occurrence of two parallel structural transformation processes with different rate constants corresponding to increasing (vesicular mixture  $\rightarrow$  onion  $\rightarrow$  cubic/lamellar/cubic three-phase nanoparticle) or decreasing interfacial curvature (inverted hexagonal  $\rightarrow$  onion  $\rightarrow$  cubic/lamellar/cubic three-phase nanoparticle) transitions. We established that (i) bound BDNF may increase the curvature of flat membrane structures, and (ii) reduce the curvature of the tubular ( $H_{II}$ -phase) lipid structures. As a result, the fluid lipid membranes change their shape and structural organization in response to the neurotrophin binding and trafficking along the

lipid/water interfaces (Figure 7). It should be taken into account that the lipid bilayers are of a flexible nature, while the neurotrophic protein has a relatively stiff  $\beta$ -sheet conformation (Figure 1a). Thus, the lipid/water interfaces adopt states of continuously changing curvatures, which most properly fit to the protein conformation and charges under the dynamic conditions of protein crowding (Figure 1d).

The proposed here structural methodology enabled *in situ* monitoring of the generation of complex membrane topologies and nanoarchitectures, in which the neurotrophic protein dynamically modified the membrane curvature through mechanisms that involve interplay of both lipid and BDNF contributions. It is essential to evoke that the bicontinuous cubic membrane architectures are generated by repeated saddle-shape bilayer membrane elements forming intertwined networks of channels.<sup>1-4,13</sup> Our structural study shows that this channel network architecture appears to be the most favorable membrane state for the BDNF trafficking. In addition, cubic membranes have been demonstrated to represent function-related shapes in cells and tissues.<sup>1,29</sup> They have fundamental significance for the membrane protein crystallization.<sup>50,52</sup> Because high membrane curvatures are inherent for trafficking intermediates,<sup>22</sup> it could be suggested that the obtained BDNF-loaded cubic membrane assemblies may constitute a potentially efficient multicompartiment nanosystem for delivery of neurotrophins.

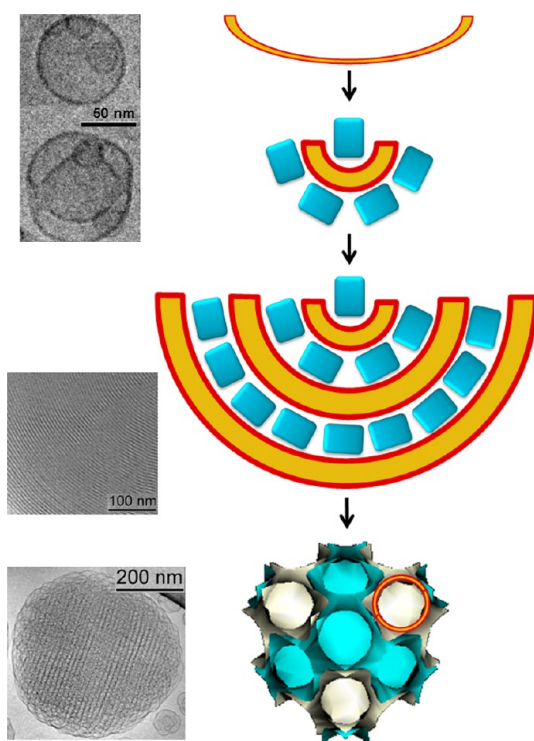


**Figure 7. Pathway of stepwise curvature changes occurring upon dynamic ordering and assembly of neurotrophin BDNF with flexible lipid membranes. The discrete jumps of curvature, leading to nanochanneled architecture formation, are determined by the rigid  $\beta$ -sheet structure of the neurotrophic protein molecules (represented as stiff cylinders).**

Recently, Zabara *et al.*<sup>6,45</sup> have reported the reconstitution of a pore-forming transmembrane protein OmpF (the outer membrane protein F) in a bicontinuous cubic lipid phase and in an inverted hexagonal lipid phase under equilibrium conditions. These studies have emphasized that the protein OmpF, reconstituted at concentrations in the range from 0.1 to 0.5 wt %, retains its functional activity in the bulk lipid mesophases. Moreover, no evidence for structural phase transitions of the host liquid-crystalline lipid matrices has been found by X-ray diffraction measurements performed at such membrane protein concentrations.<sup>6,45</sup> Indeed, the concentration of the reconstituted membrane protein should be higher in order to provoke the nucleation of membrane protein crystals in the lipid mesophase accompanied by a cubic-to-lamellar phase transition under the influence of appropriate crystallization screen.<sup>52</sup>

Our work suggests that the water-soluble signaling protein BDNF, because of its nonflexible  $\beta$ -sheet conformation, appears to be a modulator of the membrane curvature at the millisecond time scale. The neurotrophin is capable to induce bicontinuous cubic

phase architectures (characterized by nanochanneled network topologies) upon uploading in supple membrane carriers. The protein transfer from the aqueous surrounding into the lipid membrane assemblies may be as high as 82%. Taking into account that BDNF may considerably alter the interfacial curvature upon binding to lipid membranes, the initial liquid crystalline state of the carriers, to which the neurotrophin has to be administered in order to produce BDNF-loaded cubosomes, should certainly be different from a bicontinuous cubic lipid phase architecture. Here, unilamellar lipid membrane vesicles of a chosen biomimetic composition were proven as suitable starting building blocks for the “bottom-up” assembly of protein-loaded multicompartiment cubic lipid nanoparticles.

## CONCLUSION

The obtained here structural findings provide substantial biophysical experimental support to the recent concepts about the role of proteins in modulating transient and sustained membrane curvatures.<sup>18–22</sup> Highly charged locally administered pro-survival neurotrophic proteins provoke changes in the membrane topology, which may lead to altered performance of functions and unexploited trafficking pathways. A hypothesis can be raised that the neurotrophin BDNF, under the recommended conditions of local delivery,<sup>67</sup> may act not only through biochemical signaling pathways but also as a curvature-modulating molecule. Therefore, perspective strategies for treatment of neurodegenerative and neuropsychiatric disorders should consider targeting of neuronal plasticity, survival, and synaptic regeneration through a combination of both biochemical (intracellular signaling) and physical (membrane curvature and membrane elasticity) mechanisms.

On the other hand, the efficient protein loading in the multicompartiment lipid nanocarriers and the mesostructure formation, achieved within milliseconds, suggest a perspective way toward nanocrystallization<sup>73</sup> *via* membranous assemblies. The reported millisecond kinetics of protein loading revealed the sequence of mesostructure formations preceding the nucleation. The protein-triggered cubosomal membrane assemblies comprise a highly hydrated shell and an internal normal-type bicontinuous cubic lattice domain, which is epitaxially connected to a lamellar core. These membrane architectures enable up to 82% protein upload. On the basis of these results, a unified approach for protein loading and ordering in nanostructured lipid carriers can be proposed toward advancement in membrane and amphiphile nanoarchitectonics.

## EXPERIMENTAL SECTION

**Materials and Lipid Nanosystem Preparation.** Recrystallized powder of 1-monoleoyl-rac-glycerol (MO, C18:1c9), d- $\alpha$ -tocopherol

poly(ethylene glycol) 1000 succinate (V<sub>1000</sub>) (waxy solid), and *cis*-5,8,11,14,17 eicosapentaenoic acid (20:5) (oil phase) were purchased from Sigma-Aldrich. Buffer solutions were prepared

using Milli-Q water of resistivity 18.2 MΩ cm (Millipore Co.), the inorganic salts  $\text{NaH}_2\text{PO}_4$  and  $\text{Na}_2\text{HPO}_4$  (p.a. grade, Fluka), and 2,6-di-*tert*-butyl-4-methylphenol (BHT) as an antioxidant (Sigma-Aldrich). Liquid crystalline membrane phases were self-assembled from monolein and eicosapentaenoic acid in excess buffer medium. It was considered that the eicosapentaenoic acid (EPA), as member of the family of the  $\omega$ -3 polyunsaturated fatty acids (PUFAs) may influence the bilayer elasticity and favor the formation of flexible membrane nanostructures. PEGylation was done by incorporation of a small amount of the amphiphilic derivative  $V_{1000}$  in the lipid mixture. The solvent was evaporated under flux of  $\text{N}_2$  gas. Nanostructured dispersions of lipid particles were obtained by the method of hydration of a dry lipid film followed by physical agitation of the MO/EPA/ $V_{1000}$  system. Carrier-free human recombinant brain-derived neurotrophic factor (BDNF) (13.5 kDa,  $pI = 10.5$ ) was purchased by R&D Systems and lysozyme (lyophilized powder, L6876) from Sigma-Aldrich. A protein model of BDNF (lysozyme),<sup>74,75</sup> with nearly same molecular weight and number of cationic groups, was employed for development of the methodology of the structural SAXS measurements.

**Synchrotron Radiation Small-Angle X-ray Scattering Coupled to a Rapid-Mixing Stopped-Flow Device.** Rapid mixing of equal volumes (100  $\mu\text{L}$ ) of lipid nanoparticles and protein solution was performed by a stopped-flow apparatus SFM-400 (Bio-Logic, Claix, France) mounted in the X-ray beam environment. The reactant solutions were degassed. The scattering cell consisted of a quartz capillary (1.5 mm diameter, wall thickness 10  $\mu\text{m}$ ). The test of the quality of mixing and calibration of the stopped-flow dead time were performed by the method described elsewhere.<sup>59</sup> The flow time used for rapid mixing of the two reactant solutions was 50 ms, during which the kinetic time was equal to the dead time of the stopped-flow device ( $\sim 2.5$  ms). The kinetic time evolved above this dead time upon cessation of the flow, and the first 4 ms SAXS frame was acquired during the final phase of the flow corresponding to the earliest structural signal accessible.

Small angle X-ray scattering experiments were performed at the ID02 beamline<sup>61</sup> of the European Synchrotron Radiation Facility (Grenoble, France). The X-ray wavelength and sample-to-detector distance were 0.1 nm and 1.5 m, respectively, corresponding to an accessible  $q$ -range of 0.07 to 3.2  $\text{nm}^{-1}$ . The time-resolved 2D SAXS patterns were recorded using a high-sensitivity low noise CCD detector (FReLoN 4M) having an active area of 100 mm  $\times$  100 mm, which was divided into 512  $\times$  512 pixels with 4  $\times$  4 binning. The data acquisition sequence was hardware triggered by the stopped-flow device. Each SAXS pattern was integrated over 4 ms as defined by a tandem X-ray shutter, and the readout time of the CCD detector was about 190 ms. The incident and transmitted beam intensities were recorded simultaneously with every SAXS frame. The dead time between the frames ( $\sim 190$  ms) was filled by means of a sequential data acquisition scheme in which the stopped-flow mixing sequences were repeated many times, and the successive SAXS data acquisitions were progressively delayed in steps of 4 ms. This scheme allowed to check the kinetic reproducibility and robustness of the data and, in addition, avoided the radiation damage that would have been a serious problem in the case of continuous exposure to the X-ray beam ( $4.7 \times 10^{13}$  photons/sec). Steady-state SAXS patterns were recorded using a flow-through capillary cell with data acquisition time of 100 ms.

After each data acquisition sequence, the obtained 2D images were corrected for dark current, detector spatial response function, etc., and normalized to absolute intensity unit. Normalized 2D patterns were subsequently azimuthally averaged to obtain the 1D scattering curves. Multiple patterns (20–30) of the scattering background from the quartz capillary and the solvent were measured and processed in the same way, averaged, and subtracted from the time-resolved data using the SAXS Utilities software ([www.sztucki.de/SAXSutilities/](http://www.sztucki.de/SAXSutilities/)).

The millisecond kinetics pathways, monitored by the acquisition of TR-SAXS during consecutive rapid-mixing shots, were revealed by analysis of about 670 SAXS frames. The exposure time of 4 ms represents a state-of-the-art feature in the

performed real-time investigation of the structural dynamics of the soft-matter membranous systems.

**SAXS Data Fitting and Analysis.** *Scattering from a Bicontinuous Inverted Cubic Phase.* The model of Clerc and Dubois-Violette<sup>76</sup> and Garstecki and Holyst<sup>77</sup> was used to determine the structural parameters of the double diamond inverted cubic lattice structure and the average water channel diameter,  $D_w$ . In this model, the lipid bilayer thickness,  $L$ , in the cubic lipid membrane is assumed to be a constant throughout. The intensity of the cubic phase peaks is given by

$$I(q) = \frac{c_1}{q^2} \sum_{hkl} \exp \left[ \frac{(q - q_{hkl})^2}{2\sigma^2} \right] I_{hkl} \quad (1)$$

where the peak positions are denoted by  $q_{hkl}$ , the peak widths for all peaks of the inverted cubic phase are considered to be the same and described by  $\sigma$ . The cubic phase individual peak intensities are given by  $I_{hkl}$ . The model scattering intensities are defined as

$$I_{hkl}(L) = M_{hkl} \left[ F_{hkl}^{S^*} \frac{\sin[\alpha_{hkl}\pi(h^2+k^2+l^2)^{1/2}L^*]}{\alpha_{hkl}2\pi(h^2+k^2+l^2)^{1/2}} \right]^2 \quad (2)$$

where  $L^* = L/a$  is the dimensionless lipid layer thickness,  $a$  is the unit cell parameter,  $F_{hkl}^{S^*}$  is the dimensionless structure factor,  $M_{hkl}$  is a multiplicity factor, and  $\alpha_{hkl}$  are correction parameters for a particular cubic lattice. Having done the fitting for  $L$ , the value of  $D_w$  was determined from the relationship  $D_w = 0.707a - L$ . Our nonlinear least-squares fitting algorithm is based on the known Levenberg–Marquardt method.

**Cryogenic Transmission Electron Microscopy (Cryo-TEM).** For cryo-TEM studies, a sample droplet of 2  $\mu\text{L}$  was put on a lacey carbon film covered copper grid (Science Services, Munich, Germany), which was hydrophilized by glow discharge for 15 s. Most of the liquid was then removed with blotting paper, leaving a thin film stretched over the lace holes. The specimens were instantly shock frozen by rapid immersion into liquid ethane and cooled to approximately 90 K by liquid nitrogen in a temperature-controlled freezing unit (Zeiss Cryobox, Zeiss NTS GmbH, Oberkochen, Germany). The temperature was monitored and kept constant in the chamber during all the sample preparation steps. After the specimens were frozen, the remaining ethane was removed using blotting paper. The specimen was inserted into a cryo transfer holder (CT3500, Gatan, Munich, Germany) and transferred to a Zeiss EM922 Omega energy-filtered TEM (EFTEM) instrument (Zeiss NTS GmbH, Oberkochen, Germany). Examinations were carried out at temperatures around 90 K. The TEM instrument was operated at an acceleration voltage of 200 kV. Zero-loss-filtered images ( $\Delta E = 0$  eV) were taken under reduced dose conditions (100–1000 e/nm<sup>2</sup>). The images were recorded digitally by a bottom-mounted charge-coupled device (CCD) camera system (Ultra Scan 1000, Gatan, Munich, Germany) and combined and processed with a digital imaging processing system (Digital Micrograph GMS 1.8, Gatan, Munich, Germany). The sizes of the investigated nanoparticles were in the range or below the film thickness, and no deformations were observed. The images were taken very close to focus or slightly under the focus (some nanometers) because of the contrast enhancing capabilities of the in-column filter of the used Zeiss EM922 Omega. In EFTEMs, deep underfocused images can be totally avoided.

**Conflict of Interest:** The authors declare no competing financial interest.

**Acknowledgment.** The ESRF (European Synchrotron Radiation Facility, Grenoble, France) is thanked for granting SAXS beam time and Dr. T. Narayanan for the kind support to the project SC-3358 at the ID02 beamline. B.A. acknowledges the Czech Science Foundation Grant No. P208/10/1600. A.A. and S.L. acknowledge the support from ANR SIMI10 Nanosciences and LabEx LERMAT. M.D. acknowledges the support from BIMF (Bayreuth Institute of Macromolecular Research) and BZKG (Bayreuth Center for Colloids and Interfaces). Prof. P. Couvreur is specially thanked for his interest in the BDNF studies.

**Supporting Information Available:** Additional results (Figures S1–S4). This material is available free of charge via the Internet at <http://pubs.acs.org>.

## REFERENCES AND NOTES

- Almsherqi, Z. A.; Landh, T.; Kohlwein, S. D.; Deng, Y. Cubic Membranes: The Missing Dimension of Cell Membrane Organization. *Int. Rev. Cell Mol. Biol.* **2009**, *274*, 275–342.
- Hyde, S. T.; Schröder-Turk, G. E. Geometry of Interfaces: Topological Complexity in Biology and Materials. *Interface Focus* **2012**, *2*, 529–538.
- Lingwood, D.; Schuck, S.; Ferguson, C.; Gerl, M. J.; Simons, K. Generation of Cubic Membranes by Controlled Homotypic Interaction of Membrane Proteins in the Endoplasmic Reticulum. *J. Biol. Chem.* **2009**, *284*, 12041–12048.
- Almsherqi, Z.; Margadant, F.; Deng, Y. A Look Through “Lens” Cubic Mitochondria. *Interface Focus* **2012**, *2*, 539–545.
- Suteewong, T.; Sai, H.; Hovden, R.; Muller, D.; Bradbury, M. S.; Gruner, S. M.; Wiesner, U. Multicompartment Mesoporous Silica Nanoparticles with Branched Shapes: An Epitaxial Growth Mechanism. *Science* **2013**, *340*, 337–341.
- Zabara, A.; Negrini, R.; Onaca-Fischer, O.; Mezzenga, R. Bicontinuous Cubic Phases with pH-Responsive Topological Channel Interconnectivity. *Small* **2013**, *9*, 3602–3609.
- Elsabahy, M.; Wooley, K. L. Strategies Toward Well-defined Polymer Nanoparticles Inspired by Nature: Chemistry versus Versatility. *J. Polym. Sci., Part A: Polym. Chem.* **2012**, *50*, 1869–1880.
- Hales, K.; Chen, Z. Y.; Wooley, K. L.; Pochan, D. J. Nanoparticles with Tunable Internal Structure from Triblock Copolymers of PAA-b-PMA-b-PS. *Nano Lett.* **2008**, *8*, 2023–2026.
- Elsabahy, M.; Shrestha, R.; Clark, C.; Taylor, S.; Leonard, J.; Wooley, K. L. Multifunctional Hierarchically Assembled Nanostructures as Complex Stage-wise Dual-Delivery Systems for Coincidental yet Differential Trafficking of siRNA and Paclitaxel. *Nano Lett.* **2013**, *13*, 2172–2181.
- Manet, S.; Schmitt, J.; Imperor-Clerc, M.; Zholobenko, V. L.; Durand, D.; Oliveira, C. L. P.; Pedersen, J. S.; Gervais, C.; Baccile, N.; Babonneau, F.; Grillo, I.; Meneau, F.; Rochas, C. Kinetics of the Formation of 2D-Hexagonal Silica Nanostructured Materials by Nonionic Block Copolymer Templatting in Solution. *J. Phys. Chem. B* **2011**, *115*, 11330–11344.
- Angelova, A.; Angelov, B.; Mutafchieva, R.; Lesieur, S.; Couvreur, P. Self-Assembled Multicompartment Liquid Crystalline Lipid Carriers for Protein, Peptide, and Nucleic Acid Drug Delivery. *Acc. Chem. Res.* **2011**, *44*, 147–156.
- Ariga, K.; Vinu, A.; Yamauchi, Y.; Ji, Q.; Hill, J. P. Nanoarchitectonics for Mesoporous Materials. *Bull. Chem. Soc. Jpn.* **2012**, *85*, 1–32.
- Angelov, B.; Angelova, A.; Papahadjopoulos-Sternberg, B.; Lesieur, S.; Sadoc, J.-F.; Ollivon, M.; Couvreur, P. Detailed Structure of Diamond-Type Lipid Cubic Nanoparticles. *J. Am. Chem. Soc.* **2006**, *128*, 5813–5817.
- Balmert, S. C.; Little, S. R. Biomimetic Delivery with Micro- and Nanoparticles. *Adv. Mater.* **2012**, *24*, 3757–3778.
- Allen, T. M.; Cullis, P. R. Drug Delivery Systems: Entering the Mainstream. *Science* **2004**, *303*, 1818–1822.
- Clogston, J.; Caffrey, M. Controlling Release from the Lipidic Cubic Phase. Amino Acids, Peptides, Proteins and Nucleic Acids. *J. Controlled Release* **2005**, *107*, 97–111.
- Ramanathan, M.; Shrestha, L. K.; Mori, T.; Ji, Q.; Hill, J. P.; Ariga, K. Amphiphile Nanoarchitectonics: From Basic Physical Chemistry to Advanced Applications. *Phys. Chem. Chem. Phys.* **2013**, *15*, 10580–10611.
- Stachowiak, J. C.; Brodsky, F. M.; Miller, E. A. A Cost-Benefit Analysis of the Physical Mechanisms of Membrane Curvature. *Nat. Cell Biol.* **2013**, *15*, 1019–1027.
- Zimmerberg, J.; Kozlov, M. M. How Proteins Produce Cellular Membrane Curvature. *Nat. Rev. Mol. Cell Biol.* **2006**, *7*, 9–19.
- Antonny, B. Mechanisms of Membrane Curvature Sensing. *Annu. Rev. Biochem.* **2011**, *80*, 101–123.
- McMahon, H. T.; Kozlov, M. M.; Martens, S. Membrane Curvature in Synaptic Vesicle Fusion and Beyond. *Cell* **2010**, *140*, 601–605.
- McMahon, H. T.; Gallop, J. L. Membrane Curvature and Mechanisms of Dynamic Cell Membrane Remodelling. *Nature* **2005**, *438*, 590–596.
- Stachowiak, J. C.; Schmid, E. M.; Ryan, C. J.; Ann, H. S.; Sasaki, D. Y.; Sherman, M. B.; Geissler, P. L.; Fletcher, D. A.; Hayden, C. C. Membrane Bending by Protein-Protein Crowding. *Nat. Cell Biol.* **2012**, *14*, 944–949.
- Groves, J. T. The Physical Chemistry of Membrane Curvature. *Nat. Chem. Biol.* **2009**, *5*, 783–784.
- Kirchhausen, T. Bending Membranes. *Nat. Cell Biol.* **2012**, *14*, 906–908.
- Zimmerberg, J.; McLaughlin, S. Membrane Curvature: How BAR Domains Bend Bilayers. *Curr. Biol.* **2004**, *14*, R250–R252.
- Lee, A. G. Biological Membranes: The Importance of Molecular Detail. *Trends Biochem. Sci.* **2011**, *36*, 493–500.
- Lee, A. G. Lipid–Protein Interactions in Biological Membranes: A Structural Perspective. *Biochim. Biophys. Acta, Biomembr.* **2003**, *1612*, 1–40.
- Deng, Y.; Almsherqi, Z. A.; Shui, G.; Wenk, M. R.; Kohlwein, S. D. Docosapentaenoic Acid (DPA) is a Critical Determinant of Cubic Membrane Formation in *Amoeba Chaos* Mitochondria. *FASEB J.* **2009**, *23*, 2866–2871.
- Angelov, B.; Angelova, A.; Garamus, V. M.; Drechsler, M.; Willumeit, R.; Mutafchieva, R.; Štěpánek, P.; Lesieur, S. Earliest Stage of the Tetrahedral Nanochannel Formation in Cubosome Particles from Unilamellar Nanovesicles. *Langmuir* **2012**, *28*, 16647–16655.
- Knorr, R. L.; Dimova, R.; Lipowsky, R. Curvature of Double-Membrane Organelles Generated by Changes in Membrane Size and Composition. *PLoS One* **2012**, *7*, e32753.
- Barauskas, J.; Johnsson, M.; Tiberg, F. Self-Assembled Lipid Superstructures: Beyond Vesicles and Liposomes. *Nano Lett.* **2005**, *5*, 1615–1619.
- Yoo, J.-W.; Irvine, D. J.; Discher, D. E.; Mitragotri, S. Bio-inspired, Bioengineered and Biomimetic Drug Delivery Carriers. *Nat. Rev. Drug Discovery* **2011**, *10*, 521–535.
- Ariga, K.; Yamauchi, Y.; Rydzek, G.; Ji, Q.; Yonamine, Y.; Wu, K.C.-W.; Hill, J. P. Layer-by-Layer Nanoarchitectonics: Innovation, Innovation, and Evolution. *Chem. Lett.* **2014**, *43*, 36–68.
- Yaghmur, A.; Paasonen, L.; Yliperttula, M.; Urtti, A.; Rappolt, M. Structural Elucidation of Light Activated Vesicles. *J. Phys. Chem. Lett.* **2010**, *1*, 962–966.
- Han, Y.; Shchukin, D.; Yang, J.; Simon, C. R.; Fuchs, H.; Moehwald, H. Biocompatible Protein Nanocontainers for Controlled Drugs Release. *ACS Nano* **2010**, *4*, 2838–2844.
- Skorb, E. V.; Moehwald, H. Dynamic Interfaces for Responsive Encapsulation Systems. *Adv. Mater.* **2013**, *25*, 5029–5042.
- Li, G. L.; Zheng, Z.; Moehwald, H.; Shchukin, D. G. Silica/Polymer Double-Walled Hybrid Nanotubes: Synthesis and Application as Stimuli-Responsive Nanocontainers in Self-Healing Coatings. *ACS Nano* **2013**, *7*, 2470–2478.
- Volodkin, D. V.; Skirtach, A. G.; Moehwald, H. Near-IR Remote Release from Assemblies of Liposomes and Nanoparticles. *Angew. Chem., Int. Ed.* **2009**, *48*, 1807–1809.
- Yaghmur, A.; Glatter, O. Characterization and Potential Applications of Nanostructured Aqueous Dispersions. *Adv. Colloid Interface Sci.* **2009**, *147*–148, 333–342.
- Angelov, B.; Angelova, A.; Filippov, S. K.; Karlsson, G.; Terrill, N.; Lesieur, S.; Štěpánek, P. Topology and Internal Structure of PEGylated Lipid Nanocarriers for Neuronal Transfection: Synchrotron Radiation SAXS and Cryo-TEM Studies. *Soft Matter* **2011**, *7*, 9714–9720.
- Zeng, X.; Ungar, G.; Impérator-Clerc, M. A Triple-Network Tricontinuous Cubic Liquid Crystal. *Nat. Mater.* **2005**, *4*, 562–567.
- Angelov, B.; Angelova, A.; Garamus, V. M.; Lebas, G.; Lesieur, S.; Ollivon, M.; Funari, S. S.; Willumeit, R.; Couvreur, P. Small-Angle Neutron and X-ray Scattering from Amphiphilic Stimuli-Responsive Diamond-Type Bicontinuous Cubic Phase. *J. Am. Chem. Soc.* **2007**, *129*, 13474–13479.

44. Zabara, A.; Mezzenga, R. Modulating the Crystal Size and Morphology of In Meso-Crystallized Lysozyme by Precisely Controlling the Water Channel Size of the Hosting Mesophase. *Soft Matter* **2013**, *9*, 1010–1014.

45. Zabara, A.; Negrini, R.; Baumann, P.; Onaca-Fischer, O.; Mezzenga, R. Reconstitution of OmpF Membrane Protein on Bended Lipid Bilayers: Perforated Hexagonal Mesophases. *Chem. Commun.* **2014**, *50*, 2642–2645.

46. Fong, C.; Le, T.; Drummond, C. J. Lyotropic Liquid Crystal Engineering-Ordered Nanostructured Small Molecule Amphilic Self-Assembly Materials by Design. *Chem. Soc. Rev.* **2012**, *41*, 1297–1322.

47. Angelov, B.; Angelova, A.; Mutafchieva, R.; Lesieur, S.; Vainio, U.; Garamus, V. M.; Jensen, G. V.; Pedersen, J. S. SAXS Investigation of a Cubic to a Sponge ( $L_3$ ) Phase Transition in Self-Assembled Lipid Nanocarriers. *Phys. Chem. Chem. Phys.* **2011**, *13*, 3073–3081.

48. McKenzie, B. E.; de Visser, J. F.; Friedrich, H.; Wirix, M. J. M.; Boman, P. H. H.; de With, G.; Holder, S. J.; Sommerdijk, N. A. J. M. Bicontinuous Nanospheres from Simple Amorphous Amphiphilic Diblock Copolymers. *Macromolecules* **2013**, *46*, 9845–9848.

49. Dong, Y.-D.; Tilley, A. J.; Larson, I.; Lawrence, M. J.; Amehitsch, H.; Rappolt, M.; Hanley, T.; Boyd, B. J. Nonequilibrium Effects in Self-Assembled Mesophase Materials: Unexpected Supercooling Effects for Cubosomes and Hexosomes. *Langmuir* **2010**, *26*, 9000–9010.

50. Conn, C. E.; Drummond, C. J. Nanostructured Bicontinuous Cubic Lipid Self-Assembly Materials as Matrices for Protein Encapsulation. *Soft Matter* **2013**, *9*, 3449–3464.

51. Angelova, A.; Angelov, B.; Drechsler, M.; Garamus, V. M.; Lesieur, S. Protein Entrapment in PEGylated Lipid Nanoparticles. *Int. J. Pharm.* **2013**, *454*, 625–632.

52. Liu, W.; Wacker, D.; Gati, C.; Han, G. W.; James, D.; Wang, D.; Nelson, G.; Weierstall, U.; Katrich, V.; Barty, A.; et al. Serial Femtosecond Crystallography of G Protein-Coupled Receptors. *Science* **2013**, *342*, 1521–1524.

53. Yaghmur, A.; Sartori, B.; Rappolt, M. The Role of Calcium in Membrane Condensation and Spontaneous Curvature Variations in Model Lipidic Systems. *Phys. Chem. Chem. Phys.* **2011**, *13*, 3115–3125.

54. Angelov, B.; Angelova, A.; Filippov, S. K.; Narayanan, T.; Drechsler, M.; Stépánek, P.; Couvreur, P.; Lesieur, S. DNA/Fusogenic Lipid Nanocarrier Assembly: Millisecond Structural Dynamics. *J. Phys. Chem. Lett.* **2013**, *4*, 1959–1964.

55. Angelova, A.; Angelov, B.; Garamus, V. M.; Couvreur, P.; Lesieur, S. Small-Angle X-ray Scattering Investigations of Biomolecular Confinement, Loading, and Release from Liquid-Crystalline Nanochannel Assemblies. *J. Phys. Chem. Lett.* **2012**, *3*, 445–457.

56. Yaghmur, A.; Laggner, P.; Sartori, B.; Rappolt, M. Calcium Triggered  $L_0$ - $H_2$  Phase Transition Monitored by Combined Rapid Mixing and Time-Resolved Synchrotron SAXS. *PLoS One* **2008**, *3*, e2072.

57. Vandoolaeghe, P.; Barauskas, J.; Johnsson, M.; Tiberg, F.; Nylander, T. Interaction Between Lamellar (Vesicles) and Nonlamellar Lipid Liquid-Crystalline Nanoparticles as Studied by Time-Resolved Small-Angle X-ray Diffraction. *Langmuir* **2009**, *25*, 3999–4008.

58. Conn, C.; Ces, O.; Mulet, X.; Finet, S.; Winter, R.; Seddon, J.; Templar, R. Dynamics of Structural Transformations between Lamellar and Inverse Bicontinuous Cubic Lyotropic Phases. *Phys. Rev. Lett.* **2006**, *96*, 108102.

59. Gummel, J.; Sztucki, M.; Narayanan, T.; Gradzinski, M. Concentration Dependent Pathways in Spontaneous Self-assembly of Unilamellar Vesicles. *Soft Matter* **2011**, *7*, 5731–5738.

60. Jensen, G. V.; Lund, R.; Gummel, J.; Monkenbusch, M.; Narayanan, T.; Pedersen, J. S. Direct Observation of the Formation of Surfactant Micelles under Nonisothermal Conditions by Synchrotron SAXS. *J. Am. Chem. Soc.* **2013**, *135*, 7214–7222.

61. Panine, P.; Finet, S.; Weiss, T. M.; Narayanan, T. Probing Fast Kinetics in Complex Fluids by Combined Rapid Mixing and Small-Angle X-ray Scattering. *Adv. Colloid Interface Sci.* **2006**, *127*, 9–18.

62. Lund, R.; Willner, L.; Richter, D.; Lindner, P.; Narayanan, T. Kinetic Pathway of the Cylinder-to-Sphere Transition in Block Copolymer Micelles Observed *In Situ* by Time-Resolved Neutron and Synchrotron Scattering. *ACS Macro Lett.* **2013**, *2*, 1082–1087.

63. Yaghmur, A.; Rappolt, M. Structural Characterization of Lipidic Systems under Nonequilibrium Conditions. *Eur. Biophys. J.* **2012**, *41*, 831–840.

64. Graewert, M. A.; Svergun, D. I. Impact and Progress in Small and Wide Angle X-ray Scattering (SAXS and WAXS). *Curr. Opin. Struct. Biol.* **2013**, *23*, 748–754.

65. Cho, H. S.; Schotte, F.; Dashdorj, N.; Kyndt, J.; Anfinrud, P. A. Probing Anisotropic Structure Changes in Proteins with Picosecond Time-Resolved Small-Angle X-ray Scattering. *J. Phys. Chem. B* **2013**, *117*, 15825–15832.

66. Cho, H. S.; Dashdorj, N.; Schotte, F.; Gruber, T.; Henning, R.; Anfinrud, P. Protein Structural Dynamics in Solution Unveiled via 100-ps Time-Resolved X-ray Scattering. *Proc. Natl. Acad. Sci. U. S. A.* **2010**, *107*, 7281–7286.

67. Nagahara, A. H.; Tuszyński, M. H. Potential Therapeutic Uses of BDNF in Neurological and Psychiatric Disorders. *Nat. Rev. Drug Discovery* **2011**, *10*, 209–219.

68. Lu, B.; Nagappan, G.; Guan, X.; Nathan, P. J.; Wren, P. BDNF-Based Synaptic Repair as a Disease-Modifying Strategy for Neurodegenerative Diseases. *Nat. Rev. Neurosci.* **2013**, *14*, 401–416.

69. Autry, A. E.; Monteggia, L. M. Brain-derived Neurotrophic Factor and Neuropsychiatric Disorders. *Pharmacol. Rev.* **2012**, *64*, 238–258.

70. Angelova, A.; Angelov, B.; Drechsler, M.; Lesieur, S. Neurotrophin Delivery using Nanotechnology. *Drug Discovery Today* **2013**, *18*, 1263–1271.

71. Balanzá-Martínez, V.; Fries, G. R.; Colpo, G. D.; Silveira, P. P.; Portella, A. K.; Tabarés-Seisdedos, R.; Kapczinski, F. Therapeutic Use of Omega-3 Fatty Acids in Bipolar Disorder. *Expert Rev. Neurother.* **2011**, *11*, 1029–1047.

72. Angelov, B.; Angelova, A.; Papahadjopoulos-Sternberg, B.; Hoffmann, S. V.; Nicolas, V.; Lesieur, S. Protein-Containing PEGylated Cubosomes: Freeze-Fracture Electron Microscopy and Synchrotron Radiation Circular Dichroism Study. *J. Phys. Chem. B* **2012**, *116*, 7676–7686.

73. Weierstall, U.; James, D.; Wang, C.; White, T. A.; Wang, D.; Liu, W.; Spence, J. C. H.; Bruce Doak, R.; Nelson, G.; Fromme, P.; et al. Lipidic Cubic Phase Injector Facilitates Membrane Protein Serial Femtosecond Crystallography. *Nat. Commun.* **2014**, *5*, 330910.1038/ncomms4309.

74. Mehratra, S.; Lynam, D.; Maloney, R.; Pawelec, K. M.; Tuszyński, M. H.; Lee, I.; Chan, C.; Sakamoto, J. Time Controlled Protein Release from Layer-by-Layer Assembled Multilayer Functionalized Agarose Hydrogels. *Adv. Funct. Mater.* **2010**, *20*, 247–258.

75. Koennings, S.; Sapin, A.; Blunk, T.; Menei, P.; Goepferich, A. Towards Controlled Release of BDNF-Manufacturing Strategies for Protein-loaded Lipid Implants and Biocompatibility Evaluation in the Brain. *J. Controlled Release* **2007**, *119*, 163–172.

76. Clerc, M.; Dubois-Violette, E. X-ray Scattering by Bicontinuous Cubic Phases. *J. Phys. II* **1994**, *4*, 275–286.

77. Garstecki, P.; Holyst, R. Scattering Patterns of Self-Assembled Cubic Phases. 2. Analysis of the Experimental Spectra. *Langmuir* **2002**, *18*, 2529–2537.